Analysis of interface mode localization in disordered photonic crystal structure

Amit Kumar Goyal, Mudassir Husain, and Yehia Massoud*
Innovative Technologies Laboratories, King Abdullah University of Science and Technology, Thuwal, Saudi Arabia

Abstract. A disordered photonic crystal (D-PhC) structure is analyzed to study the interface mode localization characteristics. The design comprises a bilayer-disordered PhC structure, where layers are arranged in Thue–Morse sequence (TMS). The impact of local symmetric sub-structures on eigenstates coupling is also considered over a wider wavelength range. The mode hybridization study is carried out for varying refractive index contrast values of TMS structures at an operating wavelength of 550, 632.8, and 750 nm, respectively. The dispersion analysis confirms the localization of bulk guided, and edge-guided modes for different incidence angles at the structural local resonators. Further, increasing the RI contrast value leads to generation of hybrid interface modes of very high electric field intensity. Thus, showing its potential applications in both sensing and light guiding applications. Moreover, because of the higher surface electric field intensity this structure can also be used for fluorescence-based detection and surface-enhanced Raman spectroscopy as well. [DOI: 10.1117/1.JNP.16.046007]

Keywords: photonic crystal; disordered photonic crystal; aperiodic structure; surface mode; Thue–Morse sequence.

Paper 22076G received Aug. 21, 2022; accepted for publication Nov. 21, 2022; published online Dec. 6, 2022.

1 Introduction

Disordered photonic devices are recently explored for various unique applications because of their inherent properties of anomalous transport and transmission spectrum.[1,2] These devices exhibit local symmetric sub-structures those leads to generation of local resonances within the bandgap,[3,4] which can further be related to interface edge modes. The occurrence of these localized interface edge modes depends on the repeated substructures and thus may also lead to topological characteristics.[5] The interface edge mode assisted metallic photonic devices have been extensively explored for various applications such as intensity improvement in harmonic generation, sensors, lasers, and wave-guiding.[6,7] The band structure of these disordered photonic devices is comparatively more complex than conventional one-dimensional photonic crystal (1D-PhC) structures.[8–11] These structures also exhibit unique collective properties, which are not possible by their constituent parts. In electronics, Anderson model is widely used to study the electron localization in disordered systems.[12,13] However, in photonic systems, coherent backscattering can be used to study the interface state localization characteristics.[14,15] Various disordered configuration such as Octonacci, Fibonacci, Thue–Morse, and Rudin–Shapiro have been investigated for topological properties.[2,16,17]

Recently in 2022, it is shown that Fibonacci-based structures possess the potential to excite the both Tamm-like interface mode and bulk-guided modes by changing the incidence angle.[18] The Thue–Morse systems (TMS) stand out among these in a unique way. TMS is considered as a link between periodic structure and Fibonacci series.[19] They are deterministic, aperiodic systems and have delocalized electronic states but lack translational invariance.[20,21] Further, it is also demonstrated that these D-PhC structures are having both traditional and fractal bandgaps, which arise because of local symmetric substructures.[21,22] Based on this, TMS-based devices

---

*Address all correspondence to Yehia Massoud, yehia.massoud@kaust.edu.sa have been explored for various unique applications such as development of narrowband filters[23] and omnidirectional reflectors.[24,25] Researchers have examined the physical characteristics of TMS-based devices, including the transmission characteristics of TMS ternary plasma PhCs,[26] two-dimensional TMS,[27] porous silicon TMS,[28] photonic quasi-crystal fiber based on the TMS,[29] Thue–Morse ordered superconducting PhCs,[30] and multicomponent TMS.[31] However, less work is carried out to distinguish the localization feasibility of various optical interface edge-states at oblique incidence angles in these disordered photonic structures, especially Thue–Morse sequence-based systems.

In this paper, localization of optical interface edge-states is analyzed for a dielectric material assisted Thue–Morse sequence based disordered photonic crystal (D-PhC) structure. The structure is designed considering a 1D-PhC structure having dielectric multilayers of silicon dioxide (SiO_2) and titanium dioxide (TiO_2) materials that are arranged in Thue–Morse sequence-based (TMS) configuration ($S_n = S_{n-1} + S^+_{n-1}, n \geq 1$). This exhibits the generation of a number of local symmetric substructures. The impact of these local symmetric substructures on eigenstates coupling is considered over a wider wavelength range. Initially, the structure is designed to have a bandgap at central wavelength of 632.8 nm. The detailed wavelength and angular interrogation are performed to study the interface mode confinement characteristics. Further, the impact of variation in index contrast of considered materials is also studied at various other wavelengths of 550 and 750 nm, respectively. This confirms the localization of interface hybrid modes for different index contrast values at different wavelengths. The modes energies are also increasing with incidence angle. The wavelength interrogation depicts that at the considered structure exhibits generation of both bulk-guided and edge-guided interface localized modes at different incidence angles. The generation of hybrid modes enables its potential applications in both sensing and light-guiding applications. Moreover, because of the higher surface electric field intensity this structure can also be used for fluorescence-based detection and surface-enhanced Raman spectroscopy, as well.[32] Additionally, the structures fabrication does not require conventional nanolithography techniques[33]. Since it is a multilayer structure without any external pattern, thus can easily be fabricated by dip-coating/spin-coating or deposition methods.[34–36]

2 Theoretical Analysis and Structure Design

The schematical representation of the considered disordered photonic crystals (D-PhC) structure based on Thue–Morse sequence (TMS) is shown in Fig. 1. Thue–Morse multilayers are aperiodic layers arranged in recursive nature. This is accomplished by a very simple relation $S_n = S_{n-1} + S^+_{n-1}$ for $n \geq 1$ with $S_0 = A$ and S^+_0 is obtained by exchanging "A" and "B," where S_n represents the nth member of the Thue–Morse series.[37] This can also be designed using the simple inflation rule: "A" changed to "AB," and "B" changed to "BA." Where, "A" and "B" are considered two materials of high (n_A) and low (n_B) refractive indices having physical thickness d_A and d_B, respectively. The schematics of considered structure for $n = 3$ Thue–Morse sequence are shown in Fig. 1. The structure is considered finite in the "z" direction.

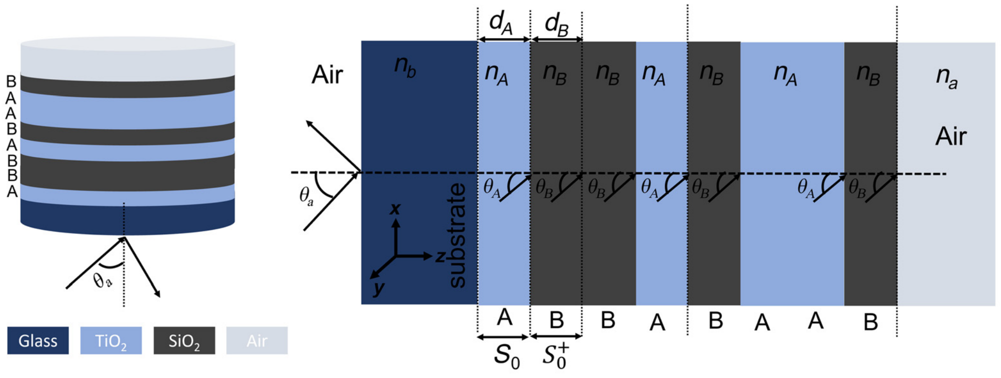

Fig. 1 Schematic representation of proposed disordered photonic crystal structure.

Table 1 The first six members of the considered D-PhC design.

S.N.	Thue–Morse series member (S_n)	D-PhC
1	S_0	A
2	S_1	AB
3	S_2	ABBA
4	S_3	ABBABAAB
5	S_4	ABBABAABBAABABBA
6	S_5	ABBABAABBAABABBABAABABBAABBABAAB

Typically, in the visible range, the thickness of the materials is calculated by the formula of ($d = \lambda/(4n)$), where λ is the central wavelength (here, 632.8 nm initially) of m'th traditional bandgap and is calculated by $2(L_A + L_B)/m$. Here, L_A ($n_A \times d_A$) and L_B ($n_B \times d_B$) are the optical lengths of the considered materials.[38] The alternate high and low refractive index sequence is used to calculate the sixth-order TMS multilayer structure thickness. The TMS sequence for $N = 6$ (up to S_5) element [1, 2, 1, 1, 2, 2, 2, 1, 1, 2, 1, 1, 2, 1, 1, 2, 2, 2, 1, 1, 2, 1] is shown in Table 1.

For the calculations, BK7 glass is considered as a substrate having refractive index of 1.515. Titanium dioxide (TiO_2) and silicon dioxide (SiO_2) are considered as material "A" and "B" having refractive indices (physical thickness) of around 2.2 (72 nm) and 1.46 (108 nm), respectively. The wavelength dependent refractive indices of both the materials ("A," "B") are calculated using Sellmeier equation and are represented by Eqs. (1) and (2).[39,40]

These materials have extremely low and constant loss factor over the complete visible spectrum (400 to 700 nm) and are well-explored to build multilayer structures. The lossy properties of these materials are considered by using their imaginary refractive index. The imaginary dielectric constants of around 0.0007i and 0.0001i are used for materials "A" and "B," respectively

$$n_A^2 = 5.913 + \frac{0.2441}{\lambda^2 - 0.0803}, \tag{1}$$

$$n_B^2 - 1 = \frac{0.6961663\lambda^2}{\lambda^2 - 0.0684043^2} + \frac{0.4079426\lambda^2}{\lambda^2 - 0.1162414^2} + \frac{0.8974794\lambda^2}{\lambda^2 - 9.896161^2}, \tag{2}$$

where n_A and n_B are the refractive indices of material and λ is the central working wavelength. The optical length (L_A and L_B) of layers is optimized to obtain an overall higher reflection. Although the proposed structure is completely disordered still the intuitive order can be introduced to ease the computation. Here, we analyze the impact of refractive index contrast variations on interface state excitations at different wavelength for TMS of $N = 6$ (S_0 to S_5) elements. For $N = 6$, the proposed TMS structure is represented by "Substrate|ABBABAABBAAB ABBABAABABBAABBABAAB|Air." This can further be simplified to "Substrate|XYYX| Air." Here, X = ABBAB AAB, Y = BAABABBA are considered as a subgroup of the D-PhC structure having "X" and "Y" as the periodic element. However, the structure can be rearranged in other subgroups as well. Furthermore, the structure can also be designed considering only two subgroups as "Substrate|PQQPQPPQ|air" having P = ABBA and Q (= P^+) = BAAB. Since the structure is finite in the "z" direction, corresponding field amplitude for TE polarized light is calculated by $E_y(x, z, t) = E_y(z)e^{i[k_n n_a \sin(\theta_a)x - \omega t]}$ having E_y as corresponding field components, n_a is the refractive index of incidence medium (here, air), θ_a is the incidence angle, and k_n is the wave vector.[41] The structure thus can be analyzed by applying transfer matrix (TMM) approach to either of the mentioned configurations. In TMM, the matrix formulation for subgroup "P" (M_P) can be considered as $M_P = M_A \mathbf{M}_{\mathrm{BA}} M_B M_B \mathbf{M}_{\mathrm{AB}} M_A$. Where M_i is the matrix notation for i'th layer and $M_{i,j}$ represents the propagation matrix for electromagnetic (EM) wave to propagate through layer "i" to "j."[24] This also leads to generation of phase shift (δ) that can be calculated by $\delta_i = \frac{\omega}{c} n d_A \mathrm{Cos}(\theta_i)$ having θ_i as the incident angle.[42] The same matric can further be formulated for subgroup "Q." Finally, by matrix formulation of the complete structure the overall transmission coefficient (T) can be calculated by $T = \frac{4}{M_n^2+2}$.[43]

3 Simulation Results and Discussion

The transmission behaviors of six elements TMS are analyzed for different refractive index contrast values of 18%, 28%, and 38%, respectively. We consider three TMS structures to work at a central wavelength of 632.8 nm, namely TMS1 with 18% index contrast ($n_A = 1.83$, $d_A = 86$ nm, $n_B = 1.46$, and $d_B = 108$ nm), TMS2 with 28% index contrast ($n_A = 2.2$, $d_A = 72$ nm, $n_B = 1.46$, and $d_B = 108$ nm), and TMS3 with 38% index contrast ($n_A = 3.3$, $d_A = 48$ nm, $n_B = 1.46$, and $d_B = 108$ nm). The local subgroups of TMS structure act as local resonator for considered index contrast values. For example, subgroup "P" can be considered as a local resonator with "BB" as a resonating cavity having "A" as the outer wall in "ABBA" configurations. Similarly, subgroup "Q" can also be considered as another local resonator with "AA" as a resonating cavity with "B" as the outer wall in 'ABBA' configurations. This results in localization of various interface states. The transmission characteristic of six element TMS structure for different refractive index contrast values at normal incidence is shown in Fig. 2(a). The structure is showing almost unity transmission and is symmetric around the central working wavelength. This is because of the 90-deg phase shift ($\delta_A = \delta_B = \pi/2$). Note that the transmission response of the structure is almost identical at different refractive index contrast values. However, the width is getting narrow with increasing index contrast value. Variation in transmission spectrum shape is because of the structural translation symmetry, where it is showing

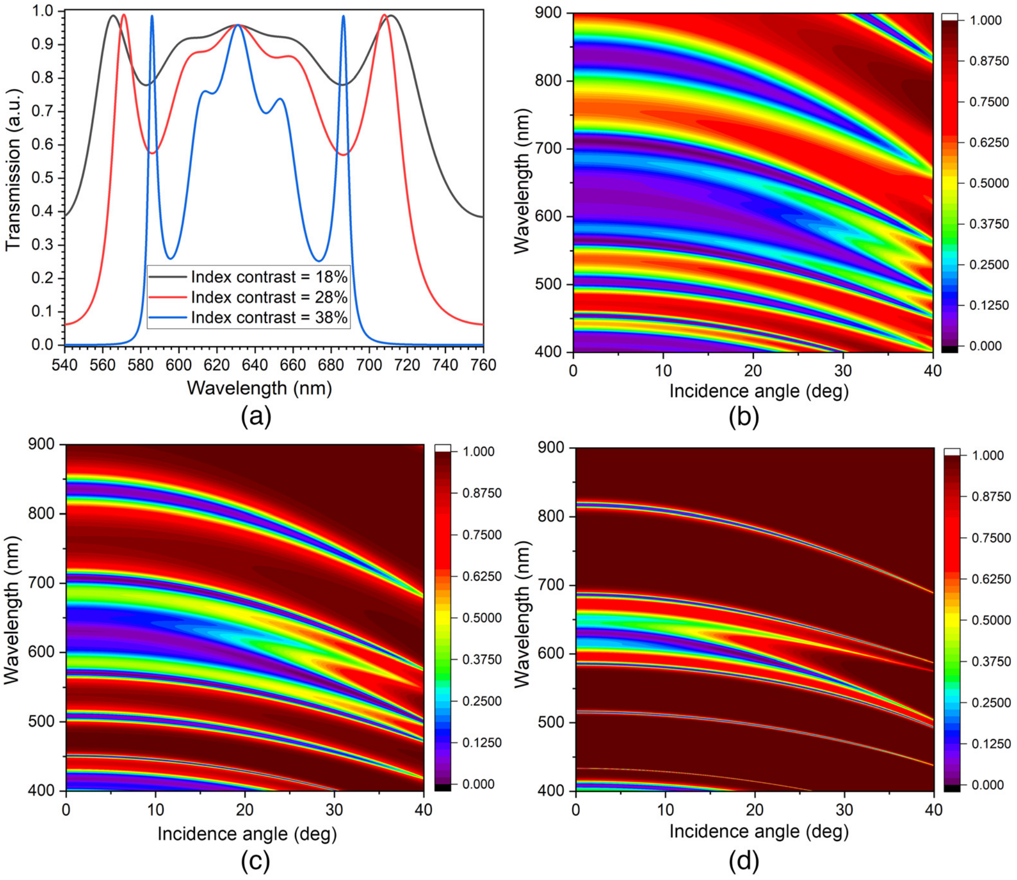

(a) (b) (c) (d)

Fig. 2 (a) Transmission spectrum of proposed QP-PhC structure at normal incidence at different index contrast values, (b)–(d) Angular reflectance dispersion diagram for corresponding index contrast 18%, 28%, and 38%, respectively.

different bandgaps for XY and YX sequence. Thus, combined effective structure XYYX results in a transmission spectrum like this.

The angular dispersion characteristics of the structure at different index contrast values are also calculated and represented in Figs. 2(b)–2(d). The analysis shows that the transmission characteristic is highly angle dependent and at the higher incidence angle the modes energies are also higher. The transmission characteristics of lower- and higher-energy modes can further be improved by increasing the elements in D-PhC structure. The localized interface states within these structures can only be analyzed for an incidence angle greater than the critical angle. Therefore, the transmission characteristic of TMS structure for $N = 6$ element at different index contrast values is analyzed beyond the critical angle (here, 41.2 deg). The angular dispersion characteristics is having more significance beyond the light line. The 3D spectral field distribution and corresponding 2D normalized electric field (obtained by using cutline along the y-directional length) of TMS having 18% index contrast value at 550 and 632.8 nm incidence wavelength is shown in Figs. 3(a) and 3(b). The cutline is shown as a dashed line in Fig. 3. For an incident wavelength of 550 nm, the structure is showing a number of interface modes, which are because of local resonator present within the TMS. As we are approaching to translation symmetry point at the mid of the structure "Substrate|XY|YX|air," a highly localized interface edge state is localized for an incidence angle of 68.8 deg at 550 nm wavelength. The mode is considered as a bulk guided mode and is represented by red curve in Fig. 3(a). Moreover, the modes those lies in bandgap are having TPP-like surface localization features. Interestingly,

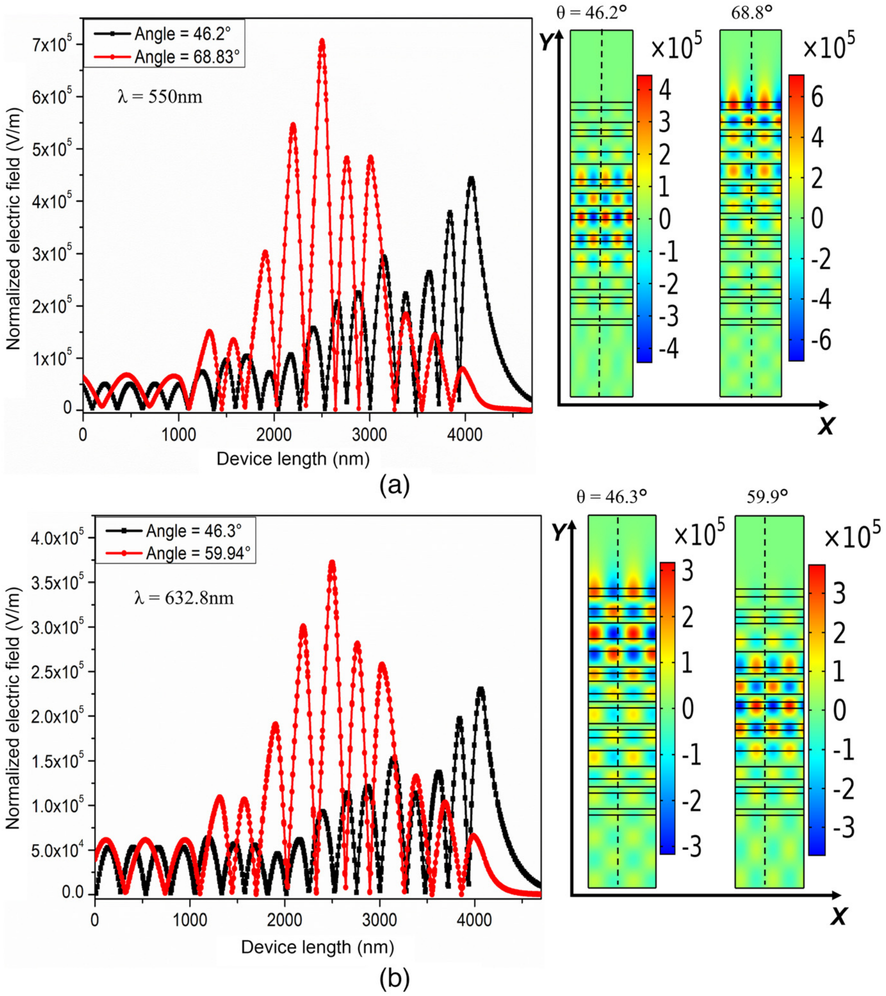

(a)

(b)

Fig. 3 Normalized surface electric field confinement along with the y-direction length of proposed structure at 18% index contrast for (a) 550 nm operating wavelength and (b) 632.8 nm operating wavelength.

decreasing the incidence angle ($\sim$46.2 deg) leads to localization of TPP-like top surface bulk guided modes [black curve in Fig 3(a)].

This can further be confirmed by analyzing its spectral field distribution. For bulk-guided mode initially, the electric field is constant within the substrate ($\sim 5 \times 10^4$ V/m), after that it attains its maximum value ($\sim 7 \times 10^5$ V/m) at the translation symmetry point and eventually decays to its original values. This leads to around 1300% increase in the E-field intensity at the local resonating subgroup. Similarly, for lower incidence angles, the structure is showing its maximum field intensity at the top interface ($\sim 4.5 \times 10^5$ V/m), which eventually decays out in the air region. Increasing the operating wavelength does not impact the interface localization location and both modes are localized at the same location within the structure but with reduced field intensities as represented in Fig. 3(b). Additionally, both type of interface state shows bulk guiding characteristics. Figure 4(a) represents the angular dispersion analysis of the TMS structure having 28% index contrast. The structure also exhibits several optical interface modes over the wavelength range of 450 to 850 nm, where most of them are the bulk-guided interface modes within the structure. Figure 4(b) represents the transmission characteristic of the considered TMS structure having 28% index contrast at 550, 632.8, and 750 nm wavelengths, respectively. For an operating wavelength of 550 nm, the structure exhibits four local minima (at 44 deg, 49 deg, 56.2 deg, and 56.86 deg), out of which only 49 deg incidence angle leads to excitation of top interface mode. The remaining three local minima corresponds to bulk interface guided modes as represented in Fig. 4(a).

The interface mode at 49 deg incidence angle is hybrid in nature. This is because the two identical local resonators in the TMS "substrate|X|YY|X|air" are sharing the same eigen energies and thus interface states are localized. Thus, the field is enhanced by the local subgroup first and then localized at the top interface. For an incidence angle of 56.2 deg, the structure supports two localized modes within the local resonators. The first one is bulk interface guided mode localized at the "substrate|X|YY|X|air" first "$X|Y$" interface and second one is the edge interface guided

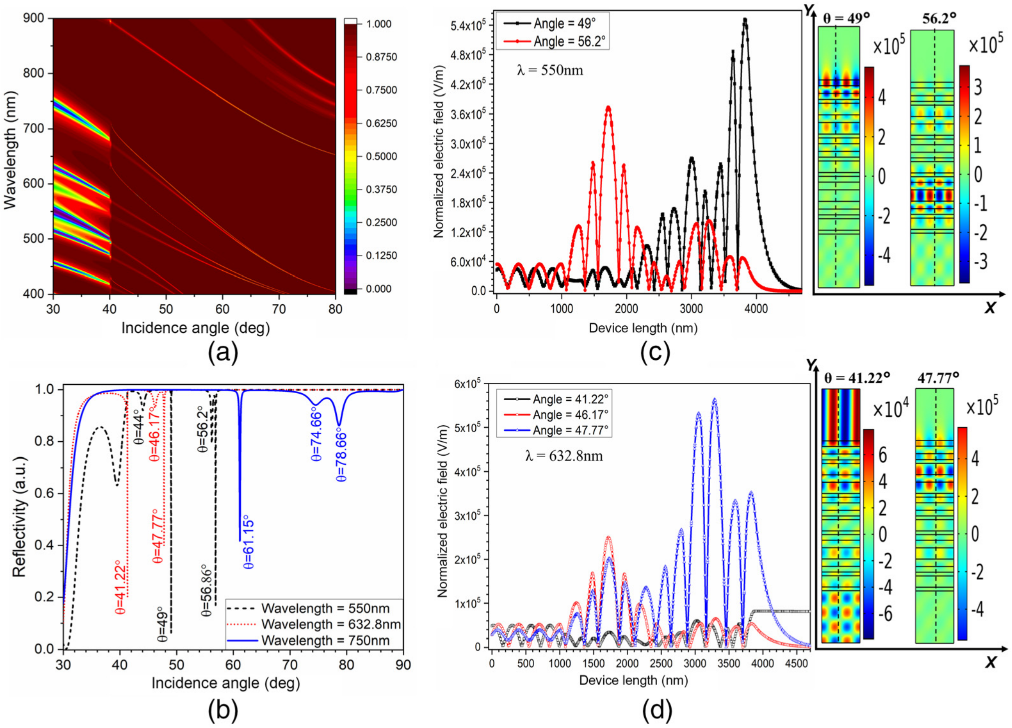

(a)

(c)

(b)

(d)

Fig. 4 Transmission characteristic of proposed structure at 28% index contrast (a) angular dispersion characteristic, (b) angular reflectance characteristic, (c) normalized surface electric field confinement along with the y-direction length of the proposed structure for 550 nm operating wavelength, and (d) normalized surface electric field confinement along with the y-direction length of the structure for 632.8 nm operating wavelength.

mode localized at the second "$Y|X$" interface. This can further be confirmed by analyzing its 3D spectral field distribution and normalized filed confinement along the y-direction as shown in Fig. 4(c). The structure is showing very high-top interface field confinement (980% higher intensity) at the incidence angle of 49 deg, whereas a bulk interface mode is excited within the structure. Furthermore, Fig. 4(d) represents the normalized surface electric field confinement along with the length of the proposed structure for 632.8 nm operating wavelength. The structure exhibits three local minima (at 41.22 deg, 46.17 deg, and 47.77 deg), out of which 47.77 deg incidence angle leads to excitation of hybrid interface mode. This is because of the interface mode has its dispersion characteristic similar to the surface mode.[44,45]

Moreover, because of the amplification at the local resonating sites, this interface mode also has good potential to be used in sensing applications. It is interesting to note that the location of structure local resonator is fixed, and interface mode are localized at those locations only. Moreover, the structure exhibits the generation of both edges guided modes and bulk guided mode. Additionally, a sharp drop at critical angle can also be observed in Fig. 4(b) at both the mentioned wavelengths. The analysis is further extended toward higher index contrast of 38% and corresponding angular dispersion analysis in presented in Fig. 5(a). The structure also exhibits several optical interface modes over the wavelength range of 450 to 850 nm, where most of them are the interface edge-guided modes within the structure. Increasing the index contrast leads to sharing the eigen energies within the local resonators, hence a number of interface states are localized. Figure 5(b) represents the transmission characteristic of the considered TMS structure having 38% index contrast at 550, 632.8, and 750 nm wavelengths, respectively. For an operating wavelength of 550 nm, the structure exhibits four local minima (at 48.48 deg, 50.57 deg, 66.3 deg, and 66.5 deg), which are representing interface edge guided states at different local substructured resonating locations as confirmed by spectral field distribution along with the length of the proposed structure and is represented in Fig. 5(c).

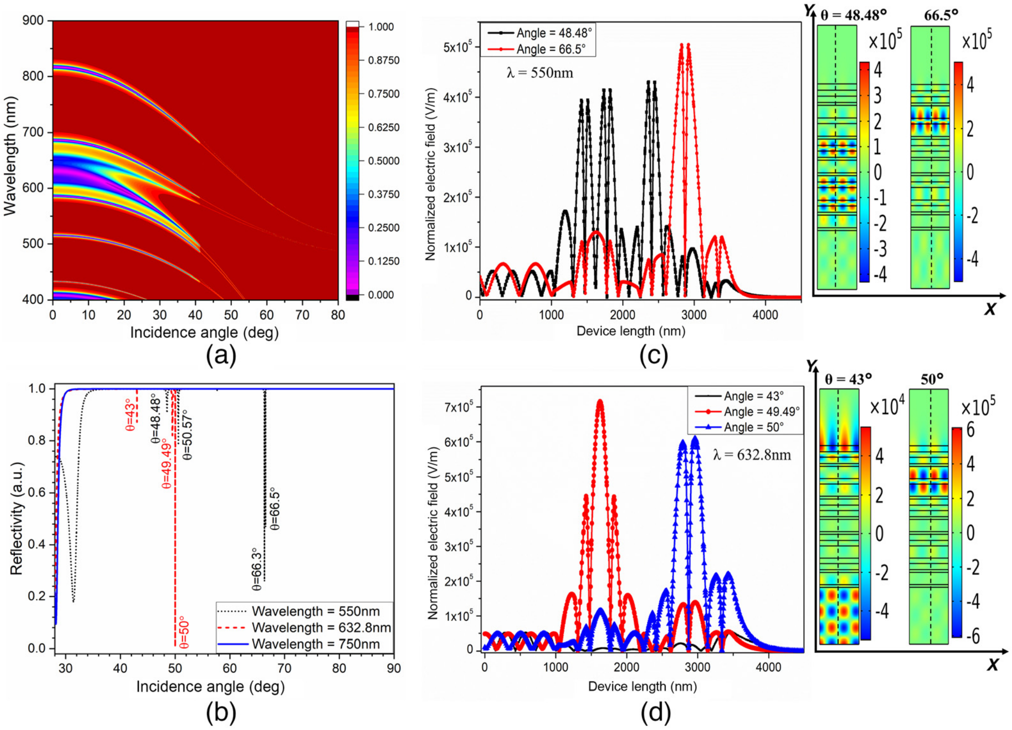

(a)
(c)
(b)
(d)

Fig. 5 Transmission characteristic of proposed structure at 38% index contrast (a) angular dispersion characteristic, (b) angular reflectance characteristic, (c) normalized surface electric field confinement along with the y-direction length of the proposed structure for 550 nm operating wavelength, and (d) normalized surface electric field confinement along with the y-direction length of the structure for 632.8 nm operating wavelength.

The structure is showing four sub-structured locations to localize interface edge states. Furthermore, Fig. 5(d) represents the normalized surface electric field confinement along with the length of the proposed structure for 632.8 nm operating wavelength. The structure exhibits three local minima (at 43 deg, 49.49 deg, and 50 deg), out of which 43 deg incidence angle leads to excitation of top interface surface mode. Moreover, the structure exhibits the generation of a number of hybrid modes including surface bulk-guided and edge guided mode. Therefore, the present structure exhibits its potential applications in both sensing and light-guiding applications. Moreover, the structure also exhibits interface energy amplification because of local subgroups, thus it can be used in fluorescence-based detection and surface-enhanced Raman spectroscopy as well.

4 Conclusion

The presented manuscript demonstrates the origin and localization feasibility analysis of various optical interface edge-states in Thue–Morse sequence-based disordered photonic crystal structure. It is observed that the structure exhibits various subgroups those results in interface state confinement at those local resonators. Depending on eigenenergy coupling at various incident angles, the structure also shows several hybrid interface modes. The structure shows a localization of strong bulk-guided mode (1300% higher field intensity) for 500 nm wavelength at 18% index contrast. Increasing the index contrast leads to generation of more hybrid modes having shared eigenenergies. This affirm the structure capability to be used in sensing, waveguiding, fluorescence imaging, and SERS applications.

Acknowledgments

The authors would like to acknowledge the research funding to the Innovative Technologies Laboratories (ITL) from King Abdullah University of Science and Technology (KAUST).

References

1. E. Maciá, “Exploiting aperiodic designs in nanophotonic devices,” *Rep. Prog. Phys.* **75**, 036502 (2012).
2. W. Gellermann et al., “Localization of light waves in Fibonacci dielectric multilayers,” *Phys. Rev. Lett.* **72**, 633 (1994).
3. S. Fan, P. R. Villeneuve, and J. D. Joannopoulos, “Large omnidirectional band gaps in metallodielectric photonic crystals,” *Phys. Rev. B* **54**, 11245–11251 (1996).
4. A. P. Vinogradov et al., “Surface state peculiarities in one-dimensional photonic crystal interfaces,” *Phys. Rev. B* **74**, 045128 (2006).
5. M. A. Bandres, M. C. Rechtsman, and M. Segev, “Topological photonic quasicrystals: fractal topological spectrum and protected transport,” *Phys. Rev. X* **6**, 011016 (2016).
6. G. Symonds et al., “Confined Tamm plasmon lasers,” *Nano Lett.* **13**, 3179 (2013).
7. S. Kumar, P. S. Maji, and R. Das, “Tamm-plasmon resonance-based temperature sensor in a Ta_2O_5/SiO_2 based distributed Bragg reflector,” *Sens. Actuators A: Phys.* **260**, 10–15 (2017).
8. M. Kohmoto, B. Sutherland, and C. Tang, “Critical wave functions and a Cantor-set spectrum of a one-dimensional quasicrystal model,” *Phys. Rev. B* **35**, 1020 (1987).
9. K. Ratra, M. Singh, and A.K. Goyal, “Design and analysis of omni-directional solar spectrum reflector using one-dimensional photonic crystal,” *J. Nanophotonics* **14**(2), 026005 (2020).
10. L. Dal Negro, *Optics of Aperiodic Structures: Fundamentals and Device Applications*, Pan Stanford, Singapore (2013).
11. A. K. Goyal, “Design analysis of one-dimensional photonic crystal based structure for hemoglobin concentration measurement,” *Prog. Electromagn. Res. M* **97**, 77–86 (2020).
12. M. Segev, Y. Silberberg, and D. Christodoulides, “Anderson localization of light,” *Nat. Photonics* **7**, 197–204 (2013).

13. C. Guan and X. Guan, "A brief introduction to Anderson localization," https://web.mit.edu/8.334/www/grades/projects/projects19/GuanChenguang.pdf (2019).
14. P.-E. Wolf and G. Maret, "Weak localization and coherent backscattering of photons in disordered media," *Phys. Rev. Lett.* **55**, 2696 (1985).
15. L. Tsang and A. Ishimaru, "Backscattering enhancement of random discrete scatterers," *J. Opt. Soc. Am. A:* **1**, 836–839 (1984)
16. C. Nayak et al., "Tunable photonic band gaps in an extrinsic octonacci magnetized cold plasma quasicrystal," *Physica B: Condens. Matter* **525**, 41–45 (2017).
17. T. Hattori et al., "Photonic dispersion relation in a one-dimensional quasicrystal," *Phys. Rev. B* **50**, 4220–4223 (1994).
18. A. K. Goyal and Y. Massoud, "Interface edge modes confinement in dielectric based quasi-periodic photonic crystal structure," *Photonics* **9**(10), 676 (2022).
19. R. Riklund, M. Severin, and Y. Liu, "The Thue–Morse aperiodic crystal, a link between the Fibonacci quasicrystal and the periodic crystal," *Int. J. Mod. Phys. B* **01**, 121 (1987).
20. S.-F. Cheng and G.-J. Jin, "Extended nature of coupled optical interface modes in Thue–Morse dielectric superlattices," *Eur. Phys. J. B-Condens. Matter* **32**, 291–296 (2003).
21. H. Lei et al., "Photonic band gap structures in the Thue–Morse lattice," *Phys. Rev. B* **75**, 205109 (2007).
22. X. Jiang et al., "Photonic band gaps and localization in the Thue–Morse structures," *Appl. Phys. Lett.* **86**, 201110 (2005).
23. S. Zirak-Gharamaleki, "Narrowband optical filter design for DWDM communication applications based on generalized aperiodic Thue–Morse structures," *Opt. Commun.* **284**, 579–584 (2011).
24. H.-F. Zhang, S.-B. Liu, and X.-K. Kong, "Enlarged omnidirectional photonic band gap in one-dimensional ternary plasma photonic crystals based on a new Thue–Morse aperiodic structure," *Solid State Commun.* **174**, 19–25 (2013).
25. K. Ratra et al., "Design and analysis of broadband reflector for passive radiative cooling," in *5th Int. Conf. Signal Process. and Commun. (ICSC)*, pp. 300 (2019).
26. L. Dal Negro et al., "Spectrally enhanced light emission from aperiodic photonic structures," *Appl. Phys. Lett.* **86**, 261905 (2005).
27. V. Matarazzo et al., "Spectral characterization of two-dimensional Thue–Morse quasicrystals realized with high resolution lithography," *J. Opt.* **13**, 015602 (2011).
28. L. De Stefano et al., "Optical properties of porous silicon Thue–Morse structures," *Physica Status Solidi C* **4**, 1966–1970 (2007).
29. V. Ferrando et al., "Guiding properties of a photonic quasi-crystal fiber based on the Thue–Morse sequence," *IEEE Photonics Technol. Lett.* **27**, 1903–1906 (2015).
30. C. Hu, H. Zhang, and Y. Ma, "Temperature-switchable mode selector in superconducting photonic crystals based on the Thue–Morse sequence," *J. Opt. Soc. Am. B* **37**, 287 (2020).
31. Y. Li and X. Yang, "Optical transmission through multicomponent Thue–Morse multilayers," *Opt. Commun.* **283**, 2160–2165 (2010).
32. A. Delfan, M. Liscidini, and J. E. Sipe, "Surface enhanced Raman scattering in the presence of multilayer dielectric structures," *J. Opt. Soc. Am. B* **29**, 1863 (2012).
33. A. K. Goyal et al., "Realization of large-scale photonic crystal cavity-based devices," *J. Micro/Nanolithogr. MEMS MOEMS* **15**(3), 031608 (2016).
34. E Saavedra et al., "Co/Ni multilayers ordered according to a periodic, Fibonnacci and Thue Morse sequence obtained by atomic layer deposition," *Nano Express* **1**, 020002 (2020).
35. A. K. Goyal, H. S. Dutta, and S. Pal, "Development of uniform porous one-dimensional photonic crystal based sensor," *Optik* **223**, 165597 (2020).
36. V. Yepuri, R. S. Dubey, and B. Kumar, "Rapid and economic fabrication approach of dielectric reflectors for energy harvesting applications," *Sci. Rep.* **10**, 15930 (2020).
37. M. Kohmoto, L. P. Kadanoff, and C. Tang, "Localization problem in one dimension: mapping and escape," *Phys. Rev. Lett.* **50**, 1870 (1983).
38. A. Hosseini and Y. Massoud, "Optical range microcavities and filters using multiple dielectric layers in metal-insulator-metal structures," *J. Opt. Soc. Am. A* **24**(1), 221–224 (2007).

39. I. H. Malitson, "Inter-specimen comparison of the refractive index of fused silica," *J. Opt. Soc. Am.* **55**, 1205–1208 (1965).
40. A. K. Goyal and J. Saini, "Performance analysis of bloch surface wave based sensor using transition metal dichalcogenides," *Appl. Nanosci.* **10**(11), 4307–4313 (2020).
41. A. Hosseini, H. Nejati, and Y. Massoud, "Modeling and design methodology for metal-insulator-metal plasmonic Bragg reflectors," *Opt. Express* **16**(3), 1475–1480 (2008).
42. J. C. Gutiérrez-Vega, "Geometric phase of dielectric multilayers," *J. Opt. Soc. Am. B* **37**(11), 3170–3178 (2020).
43. S. Savoia, G. Castaldi, and V. Galdi, "Optical nonlocality in multilayered hyperbolic metamaterials based on Thue–Morse superlattices," *Phys. Rev. B* **87**, 235116 (2013).
44. A. K. Goyal, A. Kumar, and Y. Massoud, "Performance analysis of DAST material-assisted photonic-crystal-based electrical tunable optical filter," *Crystals* **12**(7), 992 (2022).
45. A. K. Goyal, A. Kumar, and Y. Massoud, "Thermal stability analysis of surface wave assisted bio-photonic sensor," *Photonics* **9**(5), 324 (2022).

Biographies of the authors are not available.